Relationships between spike-free local field potentials and spike timing in human temporal cortex

Stavros Zanos, Theodoros P. Zanos, Vasilis Z. Marmarelis, George A. Ojemann and Eberhard E. Fetz

J Neurophysiol 107:1808-1821, 2012. First published 7 December 2011; doi:10.1152/jn.00663.2011

J Neurophysiol 107: 1808–1821, 2012.
First published December 7, 2011; doi:10.1152/jn.00663.2011.

Relationships between spike-free local field potentials and spike timing in human temporal cortex

Stavros Zanos,[1] Theodoros P. Zanos,[2] Vasilis Z. Marmarelis,[2] George A. Ojemann,[3] and Eberhard E. Fetz[1]

[1]*Department of Physiology & Biophysics and Washington National Primate Research Center, University of Washington School of Medicine, Seattle, Washington;* [2]*Biomedical Simulation Resource, Department of Biomedical Engineering, University of Southern California, Los Angeles, California; and* [3]*Department of Neurological Surgery, University of Washington School of Medicine, Seattle, Washington*

Submitted 22 July 2011; accepted in final form 6 December 2011

Zanos S, Zanos TP, Marmarelis VZ, Ojemann GA, Fetz EE. Relationships between spike-free local field potentials and spike timing in human temporal cortex. *J Neurophysiol* 107: 1808–1821, 2012. First published December 7, 2011; doi:10.1152/jn.00663.2011.—Intracortical recordings comprise both fast events, action potentials (APs), and slower events, known as local field potentials (LFPs). Although it is believed that LFPs mostly reflect local synaptic activity, it is unclear which of their signal components are most closely related to synaptic potentials and would therefore be causally related to the occurrence of individual APs. This issue is complicated by the significant contribution from AP waveforms, especially at higher LFP frequencies. In recordings of single-cell activity and LFPs from the human temporal cortex, we computed quantitative, nonlinear, causal dynamic models for the prediction of AP timing from LFPs, at millisecond resolution, before and after removing AP contributions to the LFP. In many cases, the timing of a significant number of single APs could be predicted from spike-free LFPs at different frequencies. Not surprisingly, model performance was superior when spikes were not removed. Cells whose activity was predicted by the spike-free LFP models generally fell into one of two groups: in the first group, neuronal spike activity was associated with specific phases of low LFP frequencies, lower spike activity at high LFP frequencies, and a stronger linear component in the spike-LFP model; in the second group, neuronal spike activity was associated with larger amplitude of high LFP frequencies, less frequent phase locking, and a stronger nonlinear model component. Spike timing in the first group was better predicted by the sign and level of the LFP preceding the spike, whereas spike timing in the second group was better predicted by LFP power during a certain time window before the spike.

electroencephalogram frequency ranges; nonlinear dynamic model

THE FOCUS OF IN VIVO, EXTRACELLULAR microelectrode recordings from the cerebral cortex has traditionally been fast electrical events, namely, single or multiple neuronal action potentials. The physiological correlates of lower frequency components of the extracellular potential, collectively called local field potential (LFP), are less clear. The LFP is thought to reflect postsynaptic potentials (PSPs) (Mitzdorf 1985), as well as afterpotentials and nonsynaptic membrane potential oscillations (Kamondi et al. 1998). It has also been suggested that fast components of the LFP may include contributions from action potential waveforms of recorded cells (Gold et al. 2006). Separating the various possible physiological correlates of LFPs is not straightforward, because spike waveforms themselves include both high- and low-frequency components, and PSPs are causally, albeit stochastically, related to neuronal firing. Elucidating the relationship between LFPs and spike timing has important implications for understanding and analyzing the integrative properties of cortical neurons in vivo, the links between single-cell and network activity, and the organization of cortical circuits. It is also important in the study of the physiological correlates of brain surface potentials recorded in electrocorticography (ECoG) (Crone et al. 2006), since ECoG is the surface manifestation of an LFP signal. Finally, this relationship is relevant to the design and implementation of LFP-based brain-machine interfaces (Andersen et al. 2004).

It is conceivable that those components of the extracellular potential that reflect local synaptic activity would be causally related to the output of the recorded neurons, i.e., action potentials. In that case, one should be able to relate certain features of the LFP to spike timing, with relatively high temporal resolution, on a probabilistic, spike-by-spike basis. A recent study (Rasch et al. 2008) showed that both LFP phase and power, at different frequencies, are useful in predicting the timing of action potentials recorded through the same electrode in primary visual cortex (V1). However, spike waveforms from the recorded cell contribute to the LFP across a range of frequencies (Fig. 1). It is therefore unclear to what extent these spike-predictive features represent input-related processes, such as PSPs, versus spike-related "artifacts." Moreover, V1, as well as other primary sensory cortical areas, shows a strong evoked response to sensory stimuli, and the LFP-spike relationships that have been described in such cortical areas (Katzner et al. 2009; Rasch et al. 2008) may or may not apply to association cortices, where there is virtually no evoked component in the neural activity.

In this article we attempt to characterize the LFP components that are causally associated with the occurrence of individual spikes of cells recorded through the same electrodes but are independent of the contribution of spike waveforms, and through different electrodes in close vicinity, where the LFP signal is free of spike contamination. We also describe quantitatively the relationship between those LFP components and spike timing in a way that provides insight into potential mechanisms that relate them. Finally, we study this relationship in the human temporal association cortex, an area related to human cognitive functions, including language and declar-

Address for reprint requests and other correspondence: S. Zanos, Washington National Primate Research Center, 1705 NE Pacific, I-421, Box 357330, Seattle, WA 98195-7330 (e-mail: stavroszanos@yahoo.com).

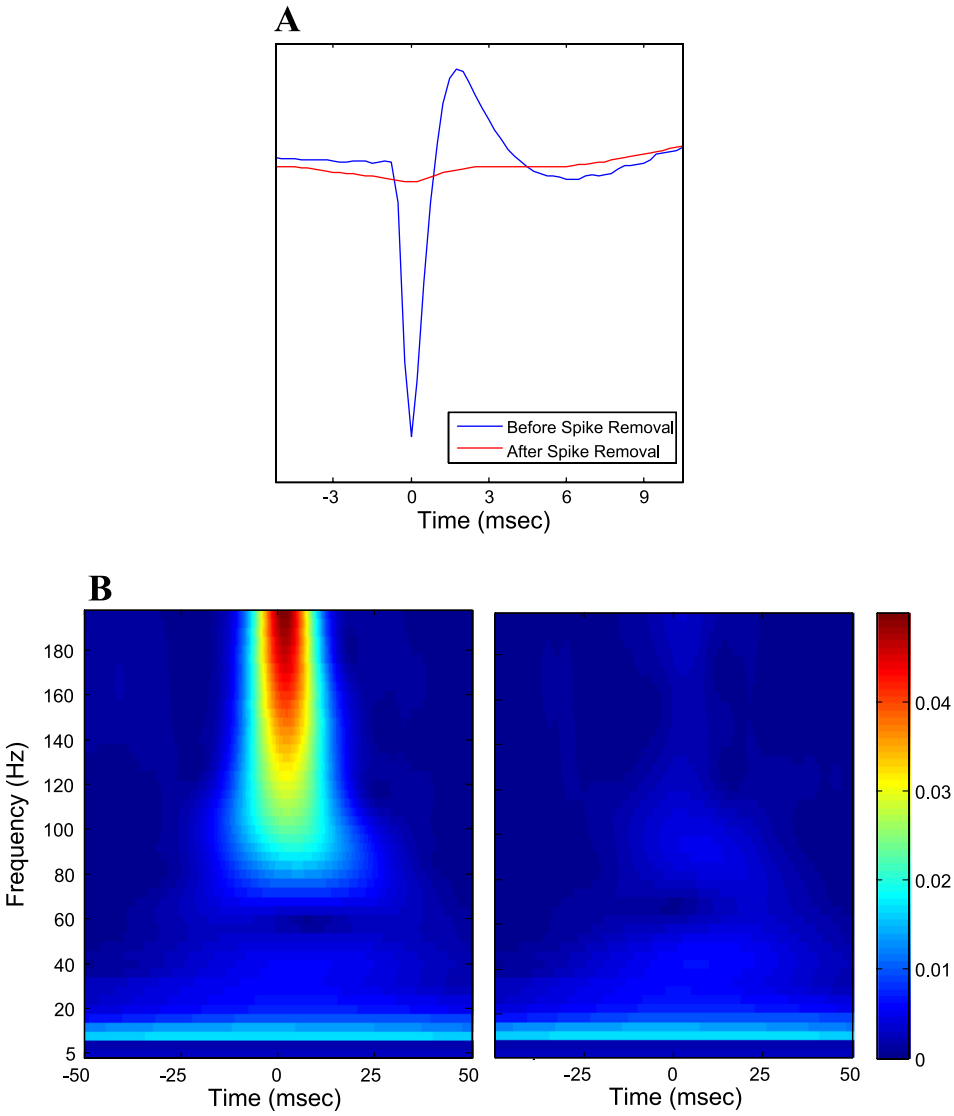

Fig. 1. Example of removal of spike waveforms from local field potentials (LFPs). *A*: spike-triggered average of LFP before (blue trace) and after (red trace) the removal of spike waveforms. *B*: spike-triggered average spectral contents of LFP before (*left*) and after (*right*) the removal of spike waveforms. Notice that power of low-frequency components (e.g., <20 Hz) has not been affected by the spike removal process.

ative memory, for which there is no physiological theory integrating single-cell and network function.

MATERIALS AND METHODS

Subject Demographics

Wide-band neural activity was recorded in patients undergoing temporal resections for medically refractory epilepsy when, for clinical reasons, the patient was awake under local anesthesia for a portion of the operation (Ojemann and Schoenfield-McNeill 1999). A total of 14 subjects (6 female) and 69 single neurons were included in the analysis. All subjects were right-handed and left-brain dominant for language based on intracarotid amobarbital perfusion testing. Mean age was 40 yr (range 25–60 yr). All but one subject had medically refractory seizures, with a mean seizure onset at age 17 yr (range 3–40 yr, 3 subjects had onsets after age 20 yr). All subjects with seizures had mesial temporal foci; four had mesial temporal sclerosis, and four gliosis. The one subject without seizures had a medial temporal benign lesion. Verbal intelligence quotient (VIQ) was available for eight subjects. Mean VIQ was 86.5 (range 72–101). Nine operations were on the left hemisphere and five on the right. The intraoperative microelectrode recording studies and the procedures for obtaining informed consent were approved by the University of Washington Institutional Review Board.

Behavioral Tasks

In 12 of 14 subjects, 3 behavioral conditions comprised the task used in this study: passive fixation, word identification (ID), and paired associated learning (PA). A detailed description of the task design is given in Ojemann et al. (2010). Briefly, during passive fixation, subjects viewed a fixation cross in the center of the screen. During the word ID task, subjects were instructed to silently read single words. During the PA task, subjects were instructed to learn a set of 15 semantically unrelated visually presented word pairs. Presentation of the word pairs was done in two blocks. In each block, the same 15 word pairs, randomly reordered, were presented over 21 s, for a total of 8 presentation cycles. In each cycle, each of the word pairs was presented for 1 s, with a 0.43-s interstimulus interval. Each of the two PA blocks was followed by a two-choice recognition task, to determine whether the subjects were actually performing the silent PA task. In the remaining two subjects, a semantic categorization task was used. During that study, subjects were shown items as either color pictures or words. Subjects were instructed to name objects in pictures or read words aloud or to say "nothing" for unnameable items.

Recordings

The microelectrode LFP recordings were obtained after completion of the surface recording and stimulation needed to plan the resection.

At that time the subject was under local anesthesia, having awakened from the propofol intravenous anesthesia used for placement of the block and craniotomy at least an hour earlier. The sites of recording were in temporal cortex that was free of interictal epileptiform discharges based on ECoG. After the microelectrode recording, this cortex was resected as part of the planned surgical resection to treat the subject's epilepsy. Other than avoiding recording from neurons with evidence of injury or epileptiform burst activity (Calvin et al. 1973), we obtained recordings from an unselected random sample of neurons at each recording site. The sites of these recordings were identified by numbered tags whose location was recorded photographically. Location of recording sites was established by the relation to the sulcal boundaries visible on those photographs (sylvian fissure, superior temporal sulcus, middle-inferior temporal gyrus sulcus) and by measurements from the recording site to the tip of the temporal lobe. Depth of the recordings was measured from the pial surface.

Two commercial tungsten microelectrodes (40-μm diameter at the shaft, sharpened to smaller tips) were back loaded through a translucent 1-cm-diameter footplate into each of two hydraulic microdrives. The footplate was used to dampen cortical pulsations. Care was taken to avoid blanching pial vessels. Two microdrives placed in lateral temporal cortex were used in all subjects. The vast majority of penetrations were performed in the superior and middle temporal gyrus. Once stable neuronal activity free from evidence of injury or epileptiform burst activity was identified (Calvin et al. 1973), the approximate cortical depth was registered and the behavioral task was initiated. The two microelectrodes on each of the two microdrives were moved separately, and in the vast majority of cases, both were inside the cortex during the recordings. The vertical distance between the two electrodes on each microdrive was registered in steps of 0.5 mm, whereas the horizontal distance was $<$1 mm, since both microelectrodes were loaded through the same 1-mm-diameter hole in the footplate. In two cases, horizontal separation was greater, because the two microelectrodes were not parallel.

The extracellular signal from each of the microelectrodes was initially amplified and then split into a "single-unit channel" (pass band 100–5,000 Hz) and an "LFP channel" (pass band 1–1,000 Hz). Analog, 60-Hz notch filters were used for both single-unit and LFP channels. All channels were digitized at a sampling rate of 10,000 samples per second (sps; or 4 ksps in 2 cases). In addition to the analog-to-digital converter, the amplified single-unit channels were routed to an oscilloscope and an audio device for real-time monitoring of neuronal activity. A personal computer system stored digitized signals, as well as timestamps and event codes of the presented stimuli.

Pairing of Spike and LFP Recordings

All analyses on all spike/LFP recordings coming from the same electrode ("single-electrode" recordings) were run twice, first on the spike-waveform-inclusive LFP and second after spike waveforms were subtracted from the LFP. A second round of analyses was performed on "dual-electrode" recordings obtained from pairs of nearby electrodes, loaded on the same microdrive, using spikes recorded on one electrode and LFPs recorded on a second electrode. In the dual-electrode cases, unit spikes, when present, were subtracted from the LFP signal before the analysis, to avoid fitting the model to spike waveforms, in addition to fitting the LFP signal.

Preprocessing of Signals

Off-line spike detection and sorting were performed manually using methodology developed by Quiroga et al. (2004). Signal-to-noise ratios (SNR) were computed for each unit, defined as the peak-to-trough voltage of the mean spike waveform divided by twice the deviation of all spike waveforms from the mean spike waveform (Kelly et al. 2007). Only units with SNRs of 2.5 or higher were included in the analysis. In addition, only recordings with at least 500 total spikes were included. Sixty-hertz noise and its harmonics were removed using third-order two-pass elliptical band-stop digital filtering.

Waveforms of individual spikes were suppressed in the original LFP signal by subtracting the spike-triggered average of the LFP, appropriately scaled and offset-corrected around each of the spike times. This ensured that ongoing LFP modulations that occurred during spikes were not altered by the spike removal process. The scaling factor for each removed spike waveform was computed as the inner product of the LFP portion that flanked that spike and the spike-triggered LFP average ($\mathrm{LFP}_{\mathrm{spike}}$) for all spikes of that unit, as shown below:

$$\mathrm{LFP}_{\mathrm{new}} = \mathrm{LFP}_{\mathrm{old}} - c \cdot \mathrm{mean}\{s_{\mathrm{w}}\}$$

where $c = \mathrm{LFP}_{\mathrm{spike}} \cdot \mathrm{mean}\{s_{\mathrm{w}}\}$, and $\mathrm{mean}\{s_{\mathrm{w}}\}$ is the mean unit spike waveform as returned by the spike-sorting algorithm.

Figure 1 shows an example of removal of spike waveforms from the LFP waveforms. This spike removal method is conceptually similar to one recently reported by one of the authors (Zanos et al. 2011); in fact, the latter reduces to the former in the case of nonoverlapping spikes, as was the case with the data in our study. The currently used method was adopted because it significantly reduced computational time. Both of the two methods were tried in a subset of our recordings (30 of 69 cell recordings). After spike removal, 10-ms-long segments of spike-free LFPs around spikes were used to compile spike-triggered LFP averages (STAs). For each of the 30 recordings, STAs from the two methods were then cross-correlated. Mean correlation coefficient (CC) was 0.9503 (range 0.91–0.98). Because CCs were computed only over very short segments around spike, their high values suggest that spike removal with the two methods is essentially identical.

Filtered versions of the LFP were produced by applying third-order two-pass elliptical bandpass digital filters at the following ranges: 4–8, 8–14, 14–30, 30–60, and 80–150 Hz. Artifact-free portions of the recording were concatenated into two data vectors, one with LFP and one with spike times, spanning the entire behavioral block. Half-second zero-padding between concatenated segments was done to avoid biases in the Volterra kernels estimation introduced by discontinuities of the concatenated signal. The length of the zero-padded segment was chosen to match the duration of the memory (length) of the kernels, which was initially set to 500 ms.

Modeling Methodology

The LFP-spike timing relationship was modeled using the Volterra method. This method is described in detail in Marmarelis (2004) and Zanos et al. (2008). Briefly, to compute up to second-order Volterra kernels for our continuous input–binary output model, the filtered versions of the LFP were used as the input and the simultaneously recorded spike trains (binary sequences), on the same or on a nearby electrode, were used as the output. This single-input/single-output Volterra model is expressed by the following set of equations:

$$u(n) = k_0 + \sum_{m=0}^{M-1} k_1(m)s(n-m) + \sum_{m_1=0}^{M-1}\sum_{m_2=0}^{M-1} k_2(m_1,m_2)s(n-m_1)s(n-m_2) \quad (1)$$

with

$$k_1(m) = \sum_{l=0}^{L-1} c_l^{(1)} L_1(m) \qquad k_2(m_1-m_2) = \sum_{l_1=0}^{L-1}\sum_{l_1=0}^{L-1} c_{l_1 l_2}^{(2)} L_{l_1}(m_1) L_{l_2}(m_2)$$

$$r(n) = \mathrm{TT}[u] \qquad \mathrm{TT}\quad [u] = \begin{cases} 1 & \text{if } u > \vartheta_{\mathrm{p}} \\ 0 & \text{otherwise} \end{cases}$$

where $\{k_0, k_1, k_2\}$ represents the zero-, first-, and second-order Volterra kernels, M denotes the memory of the model, $s(n)$ denotes the input (LFP), and $r(n)$ denotes the output (spike

train). It should be noted that these Volterra models are causal in the sense that each output sample is dependent solely on preceding input samples. Given a pair of input and output data sets, the Volterra kernels of the model can be estimated by expanding the kernels to Laguerre basis functions and by performing least-squares estimation of the Laguerre expansion coefficients (Marmarelis 1993). The lth-order Laguerre function is mathematically expressed as

$$L_l(m) = \alpha^{\frac{m-1}{2}}(1-\alpha)^{\frac{1}{2}}\sum_{k=0}^{l}(-1)^k\binom{n}{k}\binom{1}{k}\alpha^{(l-k)}(1-\alpha)^k \quad (2)$$

where α is the decay factor, also referred to as the "Laguerre pole" ($0 < \alpha < 1$), and m is the mth lag. The estimation method minimizes the mean-square error of the continuous model prediction, denoted by $u_p(n)$ in the model of *Eq. 1*, relative to the point-process output $y_p(n)$, without involving the trigger threshold (TT) operator or estimating the threshold θ_p. The estimated Laguerre expansion coefficients are used to reconstruct the estimates of the Volterra kernels. Six Laguerre expansion functions are used to estimate the Volterra kernels while the memory M of the model is selected at 125 ms. The estimation is performed using only one-quarter of the total input and output data, leaving the rest for validation purposes. Selection of the optimal alpha parameter of the Laguerre functions is based on the optimal in-sample model prediction. Considerable advantages in terms of estimation accuracy, input-output data requirements, and model complexity result from this significant reduction in the number of estimated values and model compactness (Marmarelis 1993; Zanos et al. 2008). Finally, a threshold is applied on the output of the kernel subsystem through a triggering threshold function that provides the predicted binary output $r(n)$. The threshold value is selected based on the true positive fraction (TPF) and false positive fraction (FPF) values, described below.

The constructed model is evaluated using the TPF and FPF values. A spike predicted by the model is termed a "true positive" (TP) if it coincides with an actual output spike (at the given sampling temporal resolution); otherwise it is termed a "false positive" (FP). Since the model prediction depends on the threshold value θ_p of the TT operator (which is not estimated through the Laguerre expansion method that is used for kernel estimation), various values of the threshold are applied on the continuous model prediction $u(n)$, and the quantities of TPF and FPF are computed for each value of the threshold according to the equations

$$\text{TPF} = \frac{\text{number of TP}}{\text{number of actual output spikes}}$$

$$\text{FPF} = \frac{\text{number of FP}}{\text{number of non spike events}} \quad (3)$$

When we plot the FPF value on the abscissa and the TPF value on the ordinate for each threshold value, we obtain the receiver operating characteristic (ROC) curve, a tool for assessing the performance of detection systems in the presence of noise. The ROC curve is a graphical representation of the competitive relation between sensitivity (TPF) and specificity (1 − FPF) of a binary detection/classifier as its detection threshold is varied. Selection of optimal threshold is based on the highest TPF value with a FPF value that does not exceed 0.005 (0.5%).

Interpretation of Kernel Shapes

The linear aspects of the system are captured by the first-order kernel, whose values at various time lags represent the effect of input at each lag to the output. Positive values in the first-order kernel denote a facilitatory effect of positive-valued inputs, whereas negative values represent a depressive effect of positive-valued inputs. Since only positive-valued outputs can cross the threshold to produce predicted spikes, positive values in the first-order kernel would exert a suppressive effect on negative-valued inputs. First-order kernels computed from these recordings show a negative phase that starts at 3–4 ms before the spike and extends to 7–15 ms before the spike (see Fig. 10, *top* panels).

The nonlinear aspects of the transformation are captured by the second-order kernel (see Fig. 10, *bottom* panels). The second-order kernel is symmetric with respect to the diagonal: the effect of lags (t_1, t_2) is the same as the effect of (t_2, t_1) because multiplication is commutative. The diagonal values of the second-order kernel reflect the response of the system to the power of the input signal, because they capture the effect of the squared values of the input at each time lag. Off-diagonal values respond to modulations at specific frequencies and the specific timing on which these frequencies occur. For example, a positive peak at lags (t_1, t_2) where $t_2 > t_1$ will have a facilitatory effect to the presence of an oscillation with a period of $t_2 - t_1$, happening at a lag of t_1.

Model Statistics

To establish the statistical significance of each estimated Volterra model (as the quantitative representation of a causal link between the inputs and the output) in the presence of noise or other sources of stochastic variability in the data, we utilized the Mann-Whitney two-sample statistic (MWS) (Zanos et al. 2008) that relates to the area under the curve (AUC) value of the ROC curve and can be used to test statistically whether a specific model is better than another as a binary predictor. The MWS represents the probability θ that a randomly selected sample X_i from the intermediate variable, $u_p(n)$, that corresponds to zero output will be less than (or equal to) a randomly selected sample Y_i from the values of $u_p(n)$ that correspond to spikes in the output. Essentially, the MWS represents how well these two random variables, X_i and Y_i, are separated. It has been shown that the area under the ROC curve (calculated using the trapezoidal rule) is equivalent to the MWS (Hoeffding 1948). The unbiased estimate of the MWS is the average of the samples Ψ:

$$\psi(X_i, Y_i) = \begin{cases} 1 & Y \le X \\ 0 & Y > X \end{cases} \quad (4)$$

formed by all possible pair combinations of the two sets of samples X_i and Y_i in the data record. The MWS is a U-statistic, and according to the theory developed by Hoeffding for U-statistics (Hoeffding 1948), it follows an asymptotically normal distribution with unbiased estimates of its mean and variance calculated from the data. The statistical significance of an estimated model can be thus tested against the null hypothesis of a random predictor (i.e., no causal input-output relationship).

We tested the significance of a computed model against the null hypothesis by establishing a 95% statistical significance threshold through Monte Carlo runs. To establish this threshold in the case of modeling the LFP-spikes relationship, we created surrogate data from the LFP signal after the spike removal process by using the Hilbert transform and shuffling the instantaneous phase of the signal while keeping the frequency content of the signal intact. The surrogate signal was then reconstructed by the inverse Hilbert transform. On this signal we added spike waveforms at the same times they were originally present and then performed the spike removal process, as described previously. The purpose of adding and removing spikes on the surrogate signal was to account for any potential artificial "signature" that may have been introduced by the spike removal process on the LFP itself. In the analysis of LFPs from which spike waveforms were not removed, the addition and subsequent removal of spikes was omitted. For each surrogate signal, we compute the corresponding Volterra model and calculate the MWS θ estimate. The "cutoff" value

of the MWS is established at the 95% significance level that serves as the threshold for the θ estimate obtained from the actual data. The computed model is accepted as statistically significant at the 95% level when the model's θ estimate is higher than the respective cutoff value.

Spike-LFP Phase and Amplitude Distributions

To test whether spikes preferred certain phases or amplitudes of the LFP, the instantaneous phase and amplitude of the LFP at 35 different frequencies (4 to 150 Hz) were first calculated, using the Hilbert transform on different filtered versions of every LFP recording. A single phase and amplitude value for each frequency was then assigned to each spike in that recording. By convention, a phase value of 0 deg corresponded to the trough of the cycle (depolarization). Amplitude values were normalized by the maximum for each recording, after outliers (>3 times the standard deviation of the distribution of amplitude values) were removed. Histograms of the distributions of spike phase and amplitude for different LFP frequencies across all spikes in many cases were finally compiled; we used 50 phase bins, ranging from 0 to 360 deg, and 100 amplitude bins, ranging from 0 to 100% of maximum amplitude. Histogram values were finally normalized by the corresponding histogram values expected by chance. Those "chance level histograms" were calculated by running the previous analysis steps for each recording, this time with a randomly generated spike train of 10,000 spikes, and the original LFP.

The uniformity of the distribution of spike phase values at the selected frequency ranges (4–8, 8–14, 14–30, 30–60, and 80–150 Hz) was assessed for every case, using the Rayleigh statistical test, corrected for the number of frequency ranges. A cell was considered phase-locked at a specific frequency range if the null hypothesis of uniformity of the phase distribution could be rejected at a corrected $P < 0.01$.

Spike-Field Coherence

To further quantify the tendency of spiking to occur in certain phases of the LFP at different frequencies, we calculated the spike-field coherence (SFC), as the power spectrum of the STA, divided pointwise by the sum of the power spectra of all LFP segments used to compute the STA (Fries et al. 2001). SFC ranges between 0 and 1; a value of 1 at a given frequency means that all spikes occur at the same phase for that frequency, whereas a value of 0 means that there is no preferred phase in that frequency.

Other Statistical Tests

Differences in TPFs between different subsets of cases analyzed (based on the anatomic location of cells or different behavioral conditions during which recordings were made) were tested for significance with the Pearson's χ^2 test. Differences in various features of the recordings (cell firing rate, SNR of spike waveforms, SFC, etc.) between cell groups were tested for significance with the Student's *t*-test.

To test for the presence of two separate groups of cases, in terms of TPFs at low and high LFP frequencies (TPF_{low} and TPF_{high}), the differences $TPF_{high} - TPF_{low}$ divided by the square root of 2 were first calculated, corresponding to the distances of points from the line of identity in the TPF_{high} vs. TPF_{low} scatter plot. These differences quantify the departure of model performance from that of a model performing equally well at both low and high LFP frequencies. These distances were then fitted by a Gaussian mixture model, first with one component (unimodal distribution) and then with two components (bimodal distribution). The model with the higher Akaike and Bayes information criteria (AIC and BIC, respectively) was taken to better describe the distribution of distances from identity line. In addition to TPFs at high and low frequencies, the same procedure was followed for the contribution of the second-order kernel at high and low frequencies.

RESULTS

Removal of Spike Waveforms From LFPs

Action potential waveforms were suppressed in the LFP recordings, as illustrated in Fig. 1. The SNR of spike-triggered LFPs before and after the removal procedure confirmed that the latter was effective (mean SNR before removal: 2.41; after removal: 0.0461). Spike removal from the LFP had significant effects on the LFP phase and amplitude preference of spikes, e.g., at what LFP phases and amplitudes spikes tended to occur. Before spike removal, more spikes tended to occur at the ascending limb of the high-frequency (>50 Hz) cycle and less during the descending limb (Fig. 2*A*, *top*). After spike removal, that pattern was not seen any more (Fig. 2*A*, *bottom*). Spike removal had an effect on the LFP amplitude preference of spiking, as well. Whereas no clear pattern was seen before the spike removal (Fig. 2*B*, *top*), many spikes tended to occur at intermediate amplitudes of spike-free, 15–50 Hz LFPs (Fig. 2*B*, *bottom*).

Model Performance

Single-electrode recordings. There were 69 same-electrode single-unit/LFP recordings. The model was successful at predicting the timing of a significant number of spikes in 56 cases (henceforth termed "significant cases") when spike waveforms had not been subtracted from the LFP and in 25 cases when spike waveforms had been removed. There was no effect of the anatomic site of the recording [left or right hemisphere, superior or middle temporal gyrus, superficial (<1.5 mm depth) or deep cortical layer] on whether a case was significant or not [*P* value was not significant (NS) for all comparisons]. In addition, there were no differences between significant and nonsignificant cases in spike waveform SNR, SNR of the spike-triggered average of the LFP before the spike removal (P = NS for all comparisons). Even though SNRs of spike-triggered LFPs after the spike removal were very low (<0.05), we tested whether small remnants of spikes could explain the performance of the models in the spike-free cases. SNRs for nonsignificant cases were no different from those for the significant cases (0.0453 vs. 0.04691, respectively; P = NS). In addition, in significant cases, model prediction rates were not correlated with SNR after spike removal ($r = 0.02$; P = NS). Average firing rate was significantly higher among significant cases (6.4 vs. 4.1 spikes/s, $P < 0.01$). Significant cases had greater average SFC values at the LFP frequency ranges of 4–8 and 10–14 Hz than nonsignificant cases (0.066 and 0.039 vs. 0.034 and 0.019, respectively, $P < 0.01$ for both comparisons). Average SFC values at high frequencies (>60 Hz) were not significantly different between significant and nonsignificant cases.

In significant single-electrode cases, the percentage of spikes whose timing was correctly predicted within 1 ms (henceforth termed TPF) ranged from 5% to 93% in the analysis of spike-inclusive LFPs and from 7% to 49% in the analysis of spike-free LFPs. In the rest of the cases, the model did not statistically outperform a random predictor, which

had a chance-level performance of 1.3–1.9%. Note that in all cases, both significant and nonsignificant, the FPF was, by requirement of the model construction method, below 0.5%.

Dual-electrode recordings. There were a total of 38 dual-electrode recordings, where a second electrode was present in close proximity of the electrode recording unit activity. In those cases, the model related spiking activity on one electrode with LFP on the second electrode.

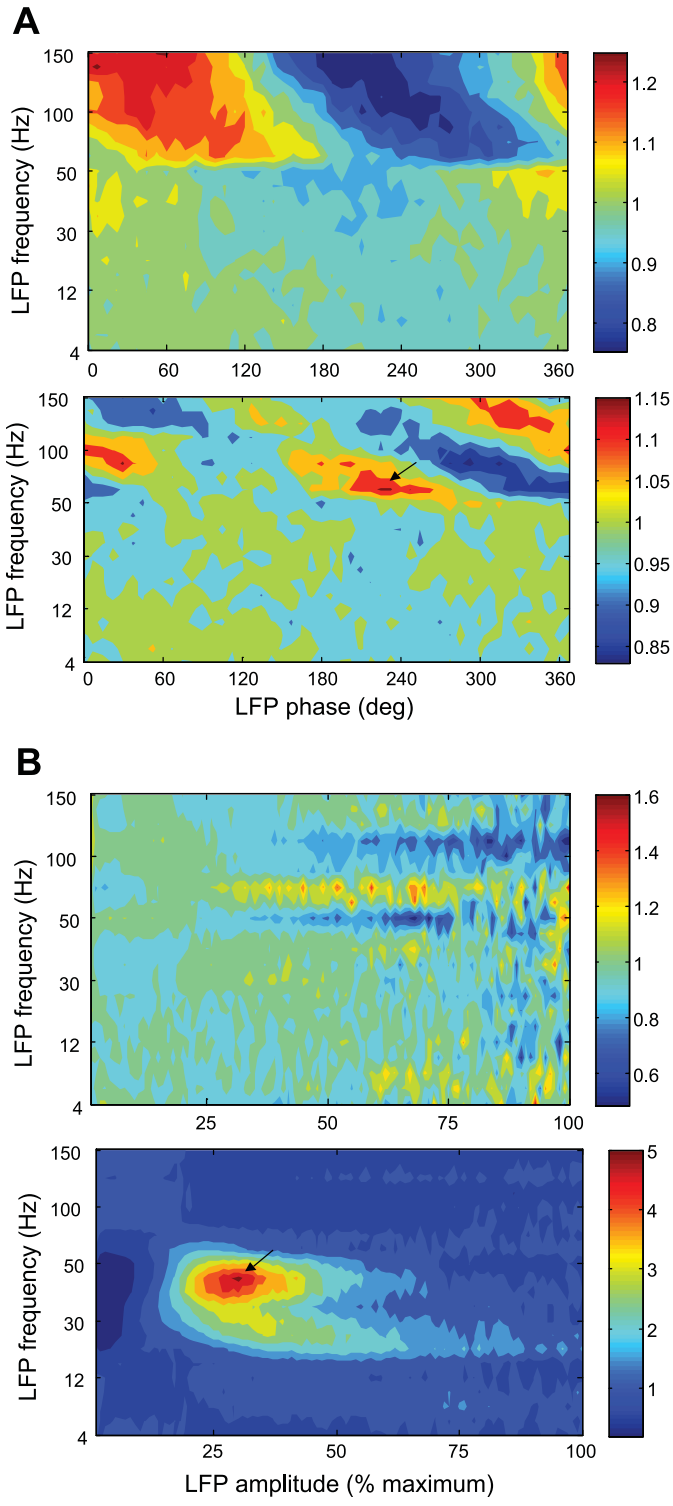

The average vertical distance between the tips of the two electrodes was 1.1 mm (range 0.5–3 mm); in 34 cases, tip distance was between 1.0 and 1.5 mm (only 5 with a distance of 0.5 mm, 1 with a distance of 3 mm). Of the 38 cases, there were 28 where models predicted the timing of a significant fraction of spikes; 22 of those 28 were "significant" in the single-electrode spike-LFP analysis, as well. In all significant cases, vertical distance of the electrode tips was ≤1.5 mm. As with the significant single-electrode cases, significant dual-electrode cases had greater average SFC values at the frequency ranges of 4–8 and 10–14 Hz than nonsignificant cases (0.052 and 0.031 vs. 0.019 and 0.011, respectively, $P < 0.01$ for both comparisons); there was no difference in SFC at high frequencies.

In significant dual-electrode cases, TPFs ranged between 3.2% and 28%. Low-frequency LFPs (4–14 Hz) were predictive of spike timing in 26 cases, medium-frequency LFPs (14–30 Hz) in 8 cases, and high-frequency LFPs (>30 Hz) in 4 cases. In each of the 28 total significant cases, the TPF was typically smaller than the corresponding single-electrode case. The average change in TPF was different for the different LFP frequency ranges used to construct the model: smaller drop for LFP frequencies 4–8 Hz and greater drop for LFP frequencies 80–100 Hz ($P < 0.001$), shown in Fig. 3 (dark gray bars).

Prediction of Spike Timing From LFPs

LFPs of different frequencies were predictive of spike timing in different recordings. Two examples of the "real-time" performance of the model on a portion of two spike-free recordings are shown in Figs. 4 and 5. In the first case, high-frequency LFP (80–150 Hz) is more predictive (Fig. 4), and the continuous model output (Fig. 4*E*) seems to be independent of the sign of changes in the LFP input (Fig. 4*D*). In this case, the linear term of the model has a weak contribution, because 87% of the predicted spikes would have been missed had the second-order kernel not been used. In the second case, low-frequency LFP (8–14 Hz) is more predictive (Fig. 5), and the model output (Fig. 5*E*) seems to follow the oscillatory changes in the LFP input (Fig. 5*D*): it peaks a little after the trough of the LFP oscillation, at a time when most spikes tend to occur. In this case, the linear term is much stronger, with only 16% contribution from the second-order kernel. This cell also shows phase-locking at the same, low-frequency, range.

Fig. 2. Preference of spiking activity for particular LFP phases and amplitudes at various LFP frequencies, before and after the removal of spike waveforms from the LFP recordings, in a total of 69 single-neuron/LFP recordings. *A*: probability of spiking, relative to that expected by chance, as a function of LFP phase at a particular frequency (abscissa) at different LFP frequencies (ordinate). By convention, a phase value of 0 corresponds to the trough of the cycle (electrode potential more negative), and a value of 180 corresponds to the positive peak (electrode potential more positive). *Top*: before the removal of spike waveforms from LFPs. *Bottom*: after the removal of spike waveforms from LFPs. Tip of arrow points to the peak of the distribution at ~220 deg at 70 Hz. *B*: probability of spiking, relative to that expected by chance, as a function of LFP amplitude, expressed as a percentage of maximum LFP amplitude at a particular frequency (abscissa), at different LFP frequencies (ordinate). *Top*: before the removal of spike waveforms. *Bottom*: after the removal of spike waveforms. Tip of arrow points to the peak of the distribution at ~30% of maximum LFP amplitude at 40 Hz. The apparent discontinuities in some of the images at around 60 Hz is due to the omission from the plots of frequencies between 55 and 65 Hz.

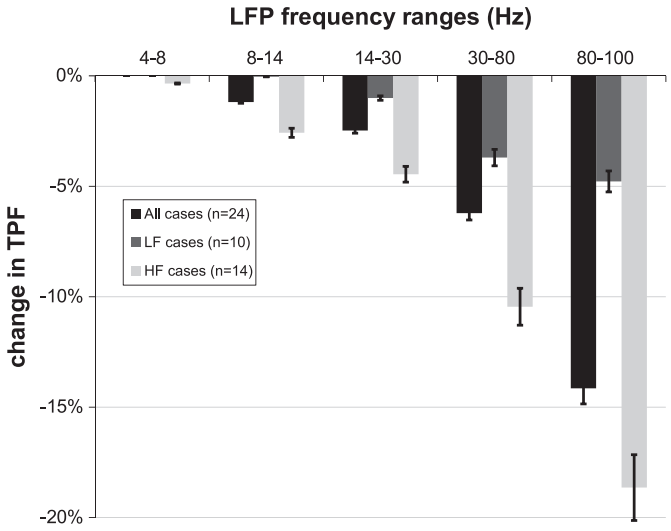

Fig. 3. Change in the performance of the spike-LFP models between single-electrode cases (unit activity and LFPs recorded on the same electrode) and the corresponding dual-electrode cases (same units, LFPs recorded on a neighboring electrode) for models computed from various LFP frequencies (4–8, 8–14, 14–30, 30–80, and 80–100 Hz) and for 3 different cell groups [all cells, low-frequency-responsive (LF) cells, and high-frequency-responsive (HF) cells]. Performance is expressed as true positive fraction (TPF; the percentage of spikes whose timing is correctly predicted by the model). Change in performance is expressed as the TPF in a dual-electrode case minus the TPF in the corresponding single-electrode case. Histogram bars indicate average TPF changes; error bars indicate standard mean errors.

Model Performance and Behavior

Subjects did indeed perform the task they were asked, since they correctly recognized the correct second word on an average of 79% of the PA items presented ($P < 0.05$ different from chance). No particular behavioral condition, among those subjects were tested on, was associated with a higher number or higher performance, as quantified by the TPF, of significant LFP-spike timing predictive models. Of the 24 recordings from which, after spike removal, predictive LFP-spike timing models were computed, the isolated cell was stable for at least two consecutive behavioral blocks (in terms of spike waveform shape, interspike interval histogram shape, and average firing rate) in 7. In most cases, (6 of 7), there was no significant change in the performance of the model between the two behavioral blocks, for all the LFP frequency ranges for which models were computed. For example, the difference in the TPF between the two behavioral conditions was, on average, less than 5% of the TPF of the first condition. Thus, when a given LFP frequency range was predictive of spike timing in the first behavioral block, the same frequency range was equally predictive in the second behavioral block. The same was true for frequency ranges that, in these same recordings, were not predictive of spike timing.

LFP Frequencies Predicting Spike Timing

Typically, successful models were computed on more than one LFP frequency range for each case. No single frequency range was associated with a larger number of significant cases. However, in significant cases, the average TPF was significantly higher for higher (80–100 Hz) LFP frequencies (33.5% and 15.2% for spike-inclusive and spike-free LFPs, respectively) than for lower (4–8 Hz) LFP frequencies (8.7% and 9.2%, respectively) (Table 1).

Significant cases formed two groups (Fig. 6*A*): *1*) the 14 so-called "high-frequency (HF) cases" had large TPFs for high LFP frequencies (80–150 Hz) and small TPFs for low LFP frequencies (4–14 Hz), and *2*) the 10 "low-frequency (LF) cases" had large TPFs for low LFP frequencies and small, or frequently nonsignificant, TPFs for high LFP frequencies. Power spectra of individual LFP recordings did not show differences in the frequencies between 4 and 150 Hz that could explain the clustering of cells into these two groups. The distribution of the difference in TPFs at low and high LFP frequencies for all significant cases (Fig. 6*A*) was better fitted by a bimodal, rather than a unimodal, Gaussian mixtures model. Unimodal and bimodal Akaike (uAIC, bAIC) information criteria were 199 and 193, respectively; unimodal and bimodal Bays criteria (uBIC, bBIC) were 205 and 194, respectively. The difference uAIC − bAIC (199 − 193 = 6) agrees with the rule of thumb that a model with AIC greater than 4 more than that of the model with the minimum AIC (considered the "best" model, the bimodal model in our case) is considerably less likely to be as good of a fit (Akaike 1980). Similarly, the Bays criteria favor the binomial model as a better fit (Schwarz 1978).

The contribution of the second-order (nonlinear) model term to the prediction performance followed a similar pattern: HF cases were associated with large contributions from the second-order kernel, and LF cases with small contributions from the second-order kernel (uAIC, 187; bAIC, 193; uBIC, 193; bBIC, 203). In addition, spikes from LF cases were more likely to have an LFP phase preference than spikes from HF cases; likewise, the contribution of the second-order kernel to the model performance was inversely proportional to the probability of phase locking to any LFP frequency range (Fig. 6*B* and Table 1, last column). Overall, among LF cases, there were more spikes with preferred LFP phases at lower frequencies than among HF cases (Fig. 7*A*). In LF cases, spikes tended to occur during times when high-frequency LFPs (>50 Hz) had low amplitude (Fig. 7*B*, *top*); in HF cases, spikes tended to occur when high-frequency LFPs had high amplitude (Fig. 7*B*, *bottom*). SFC values were different for the two groups. The LF cases had overall higher SFC values at low frequencies (4–10 Hz, $P < 0.001$), whereas at high frequencies (80–100 Hz), no significant difference between LF and HF cases was found ($P = 0.18$) (Fig. 8). In either group, SFC at low frequencies was higher than that at high frequencies ($P < 0.001$ in both cases).

The change in TPF between a single-electrode model and the corresponding dual-electrode model (same unit, LFP on neighboring electrode) was different for the two cell groups. In the LF group, there was practically no change in the TPF between the single- and the dual-electrode models for low LFP frequencies (4–14 Hz, $P = 0.19$) and moderate changes for high LFP frequencies ($P = 0.04$ for 14–30 Hz, $P = 0.01$ for 30–80 Hz, $P < 0.01$ for 80–100 Hz) (Fig. 3, medium gray bars). In contrast, in the HF group, TPFs in dual-electrode models were significantly lower than in single-electrode models at all LFP frequency ranges except 4–8 Hz, in which TPFs were very low to begin with ($P = 0.14$

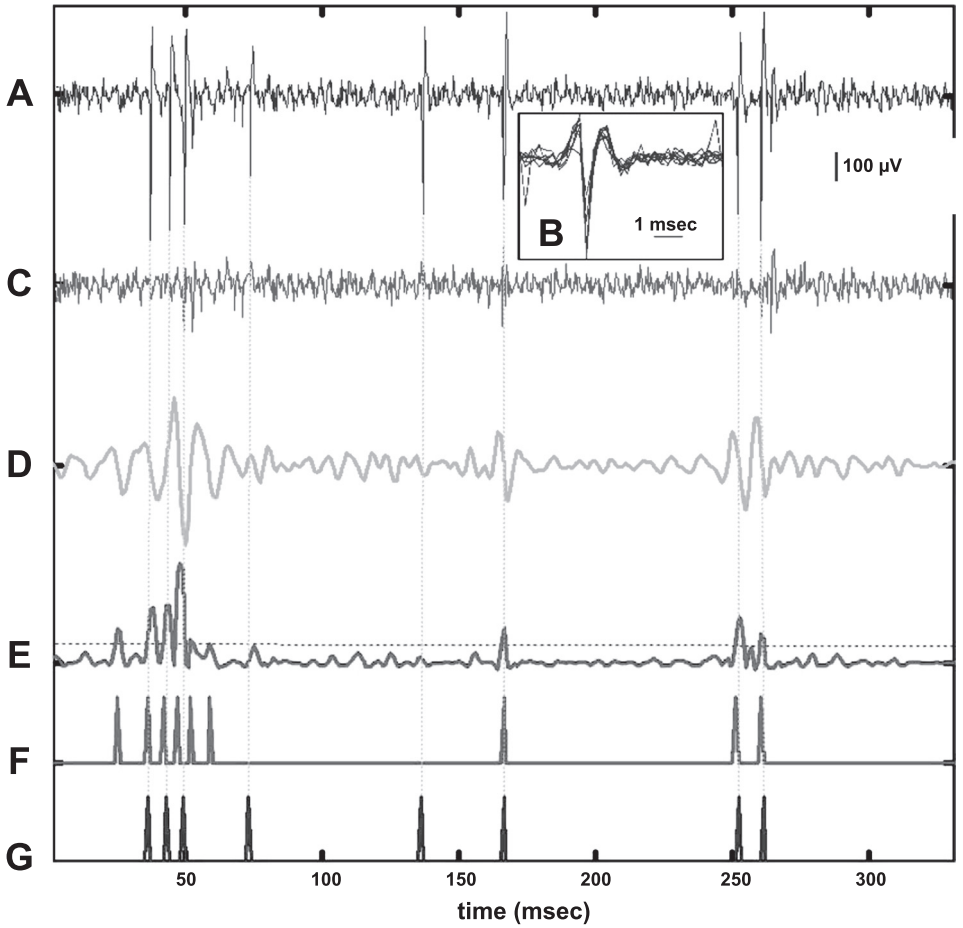

Fig. 4. Representative example of the performance of the model on a portion of a recording where high-frequency LFP (80–150 Hz) was predictive of spike timing. This recording was performed during a paired-associate learning task, 5 min after the beginning of the task. The TPF for this case was 27.8% (mean TPF for high-frequency LFP was 24.6%), the second-order contribution was 67% (mean second-order contribution was 76.7%), and the cell was not phase-locked at either low or high frequencies (only 9 of 60 cells were phase-locked to high-frequency LFPs). *A*: raw LFP signal, including several action potentials. *B*: superimposed waveforms of the isolated single-unit spikes from the recording portion shown. Vertical dotted lines denote the peaks of the spikes. *C*: LFP signal after removal of spikes. *D*: filtered version of signal shown in *C*, used as input to the model. *E*: continuous model output, calculated by the convolution of the input signal in *D* and the computed kernels. Horizontal dotted line represents the model trigger threshold. *F*: predicted spike train. *G*: actual spike train.

for 4–8 Hz, $P = 0.03$ for 8–14 Hz, $P < 0.01$ for 30–80 and 80–100 Hz) (Fig. 3, light gray bars).

We also looked for other differences between the two cell groups. There were no systematic differences in terms of spike waveform peak-to-trough amplitude or duration, interspike interval histogram type (phasic or tonic), or rhythmicity of firing, as assessed through autocorrelograms of the spike trains. There were, however, significant differences in the mean firing rates of the two cell groups in relation to the two behavioral tasks (ID and PA). Overall, LF cells were associated with lower overall firing rates than HF cells (7.2 vs. 16.75 Hz, respectively, $P < 0.01$). LF cells fired at higher rates during ID than during PA ($P < 0.01$), whereas HF cells were more active during the PA task ($P < 0.01$) (Fig. 9). That was true for mean firing rates across all cells in each group, as well as on a cell-by-cell basis; the ratio of the mean firing rate of a cell during ID to the mean firing rate of that cell during PA was 1.0566 ± 0.32 for LF cells and 0.6728 ± 0.11 for HF cells.

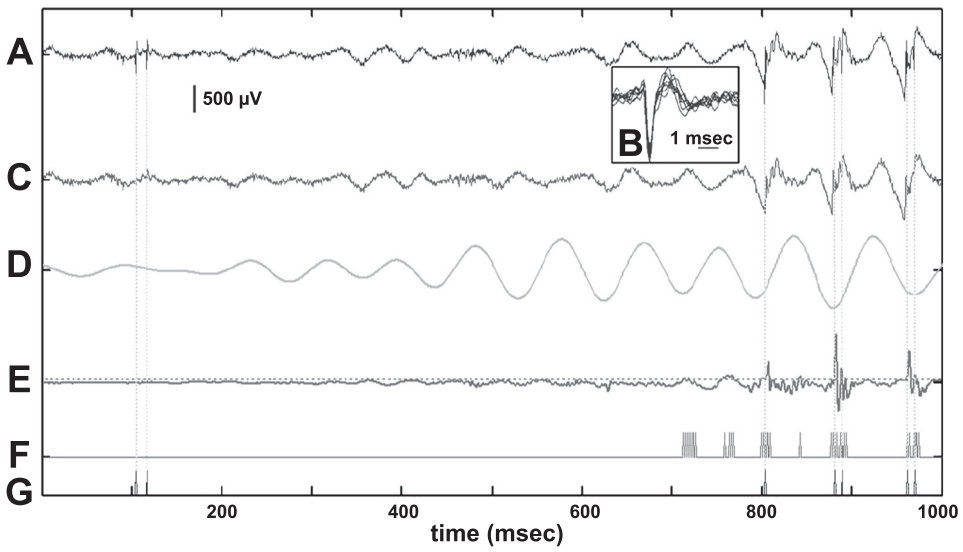

Fig. 5. Representative example of the performance of the model on a portion of a recording where low-frequency LFP (8–14 Hz) was predictive of spike timing. This recording was performed during an identification task, 7 min after the beginning of the task. The TPF for this case was 14% (mean TPF for low-frequency LFP was 19.2%), the second-order contribution was 44% (mean second-order contribution was 29.4%), and the cell was phase-locked to the ascending phase of the 8–14 Hz LFP oscillation, after the trough (22 of 55 cells were phase-locked to low-frequency LFPs). *A–G* follow the same conventions as described in Fig. 4. Note that the continuous model output (*E*) peaks at the trough of the 8–14 Hz LFP oscillation, where spikes tend to occur.

Table 1. *Summary of model performance for the different LFP frequency ranges*

Frequency Range, Hz	No. of Significant Cases (of 69 in Total)		MMP, %		No. of Cases With TPF >10%		MMP of Cases With TPF >10%		Mean Second-Order Kernel Contribution, %		Significant/Total Cases With Phase Locking
	Spike-inclusive LFPs	Spike-free LFPs	Spike-inclusive LFPs	Spike-free LFPs	Spike-inclusive LFPs	Spike-free LFPs	Spike-inclusive LFPs	Spike-free LFPs	Spike-inclusive LFPs	Spike-free LFPs	
4–8	47	24	8.7	9.2	13	9	16.6	14.2	22.5	17.7	23/60
8–14	47	24	8.7	10.4	11	8	18.0	19.2	26	29.4	22/55
14–30	50	24	9.1	9.6	14	6	17.4	17.1	34.3	51.2	16/57
30–80	46	22	11.3	12.2	18	12	20.0	20.3	35.7	73.9	12/60
80–150	52	20	33.5	15.2	43	13	40.0	24.6	44.8	76.7	9/60

For each local field potential (LFP) frequency range, the following data are provided for spike-inclusive and spike-free LFPs: the number of neurons in which the model performed statistically significant spike timing prediction and the average percentage, across those neurons, of spikes whose timing was successfully predicted within 1 ms (mean model prediction, MMP); the number of cases with a true positive fraction (TPF) above 10% and their corresponding average MMPs; and the contribution of the second-order (nonlinear) term of the model to the prediction. Finally, the number of significant and total (significant + nonsignificant) cases that showed phase locking at each frequency range are indicated.

Firing rates were calculated during the second that followed the cue for the execution of the behavioral task.

Kernel Shapes

Volterra models provide a characterization of the quantitative temporal relationship between input and output. This relationship can be represented graphically by the kernel shapes (Fig. 10), which are convolved with the input to provide the desired output. The effective memory of both first- and second-order kernels was 20 ms, beyond which time they converged to zero: LFPs more than 20 ms before the spike had no effect on spike timing.

The linear aspects of the system are captured by the first-order kernel, whose values at various time lags represent the effect of the input at each lag to the output. First-order kernels computed from these recordings show a negative phase that starts at 3–4 ms before the spike and extends to 7–15 ms before the spike (Fig. 10, *A* and *B*, *top*). The nonlinear aspects of the transformation are captured by the second-order kernel. Significant second-order effects at lags beyond 3–4 ms before the spike showed up only in the case of 80–100 Hz LFP input (Fig. 10*A*, *bottom*), where two major components are seen: high positive diagonal values of the kernel at a lag between 7 and 11 ms, and a positive-valued kernel component at the combination of lags 3 and 9–12 ms before the spike. These two components of the second-order kernel represent the combined facilitatory effect of a full 80–100 Hz oscillatory cycle in the LFP preceding a spike and of increased power in the same frequency range, occurring at the same time.

DISCUSSION

LFPs have been considered as indicators of the overall synaptic input to a cortical area, in terms of excitatory and inhibitory PSPs, from both distant and local sources, as well as voltage-dependent membrane oscillations, afterpotentials, active dendritic phenomena, etc. (Buzsaki et al. 2003; Einevoll et al. 2007; Kamondi et al. 1998; Katzner et al. 2009; Mitzdorf 1985). Intracellular recordings have shown that both low-frequency (Steriade 2004) and high-frequency (Penttonen et al. 1998) LFP modulations are closely associated with postsynaptic potentials. In addition, several studies in different cortical areas have documented the association of spiking activity with specific phases of ongoing LFP modulations at different frequencies (Feldman 1984; Jacobs et al. 2007; O'Keefe and Recce 1993). These findings suggest that LFPs should bear features that are predictive of the timing of single-unit spikes. Indeed, Rasch et al. (2008) showed that for spike-containing LFPs in the primary visual cortex, phase in low frequencies and power in higher frequencies tended to be predictive of the timing of some spikes recorded through the same electrodes.

First, we wanted to examine whether such a relationship between LFPs and spikes could be found in recordings from human temporal cortex. We also wanted to correct for two confounding effects of spike waveforms: first on high-frequency LFPs, due to the spectral overlap between the two signals, and second on the LFP-phase distribution of spikes, due to the artifactual increase in SFC from the relatively low-frequency components of action potential waveforms (Baker et al. 2003; Zanos et al. 2011). In our data set, spike waveforms did indeed affect the LFP-spike relationship, both

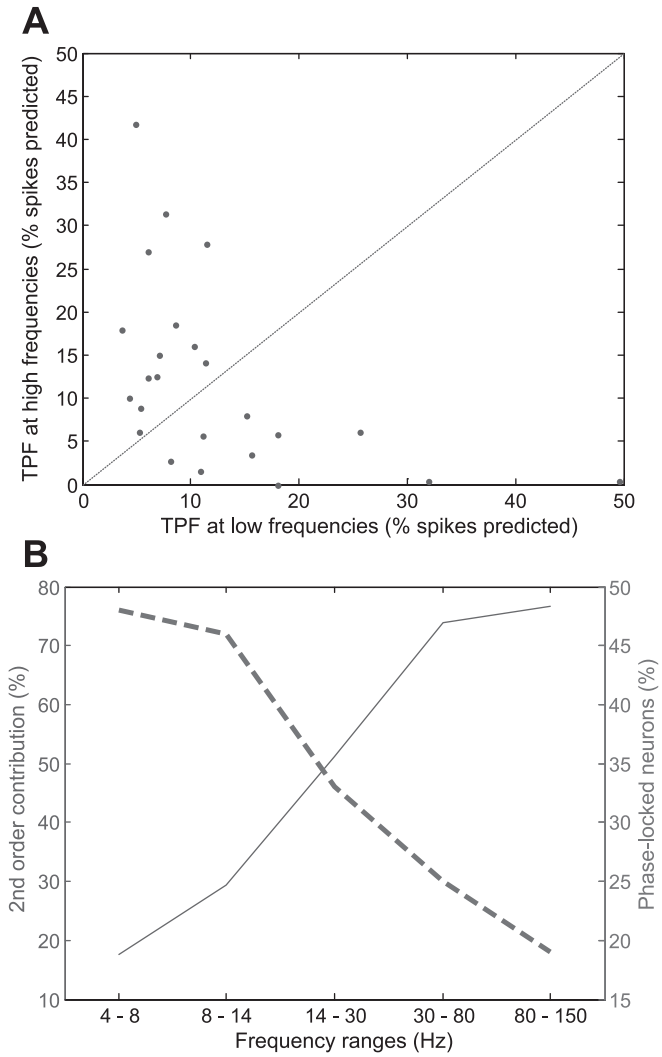

Fig. 6. *A*: TPF rates (predicted spikes as a percentage of actual spikes) at high (80–150 Hz)- vs. low (8–14 Hz)-frequency spike-free LFPs in cases where the model performance was significantly better than a random predictor. Each case is represented by a point; for points lying below the line of identity, the model performance at low frequencies is higher than that at high frequencies (14 cases in total), and vice versa for points above the line of identity (10 cases in total). *B*: average second-order contribution to the computed models across all recordings (solid line) and percentage of phase-locked cells among all cells entered in the analyses (dashed line) at different LFP frequency ranges.

spike-preferred LFP phases and amplitudes (Fig. 2). Statistically significant spike timing predictions were made in 81% of cases with spike-inclusive LFPs, with an average TPF of 33.5% at high LFP frequencies (80–150 Hz), and in 39% of cases with spike-free LFPs, with an average TPF of 15.2% (Table 1). These findings suggest that although spike waveforms themselves contribute significantly to high LFP frequencies, a considerable portion of both high- and low-frequency LFP is generated by other mechanisms and contains information that can predict the timing of a significant portion of those spikes. For these reasons, spike signatures were removed from LFP recorded on the same electrode, before the causal LFP-spike timing models were computed. Causal models between unit activity on one electrode and LFP on a neighboring electrode were also computed; in the last case, spike contamination of LFP was not an issue.

The fact that predictive models were obtained in only a subset of the recordings suggests that, at least in the temporal cortex of awake humans, not all LFPs contain information about the timing of single-unit activity recorded through the same electrode. This is consistent with the findings of Ray et al. (2008), who found that even though firing rate and high-frequency LFP power were closely matched when averaged over the entire population of recordings, the correlations were very poor on a trial-by-trial basis (for a more detailed discus-

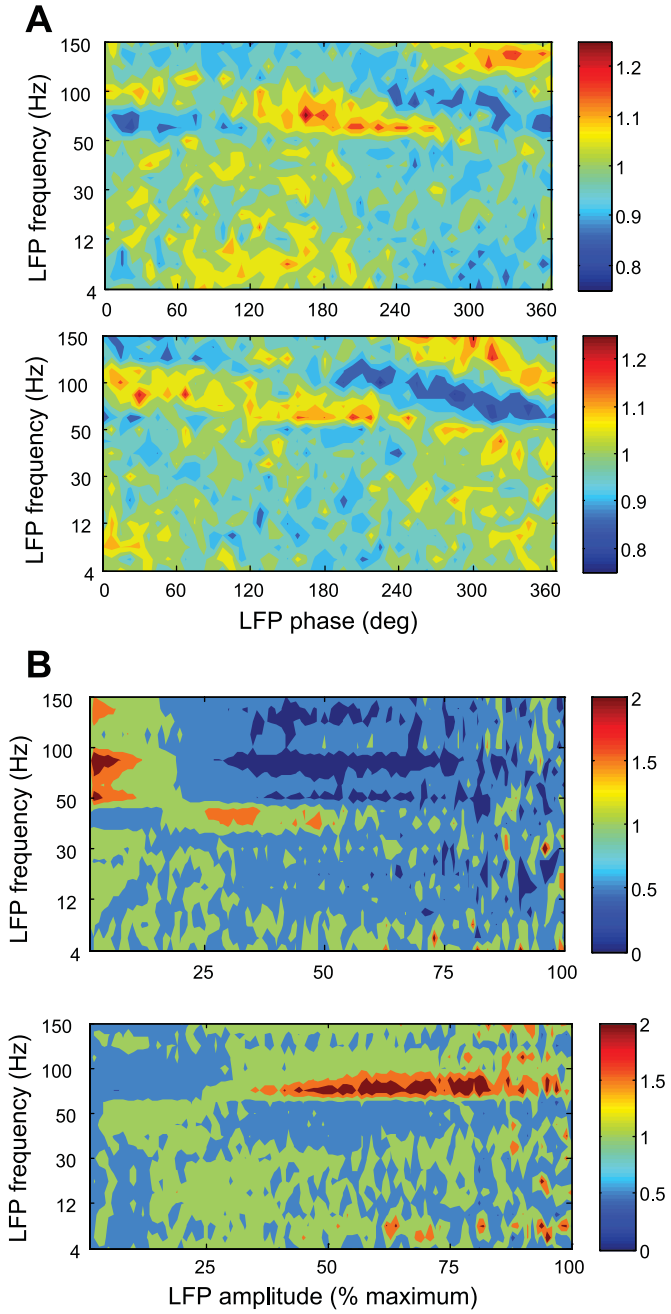

Fig. 7. Distributions of spike-free LFP phases (*A*) and amplitudes (*B*) associated with spiking activity in those cases where low-frequency LFPs were predictive of spike timing (*top* panels, total of 14 cases) and in those cases where high-frequency LFPs were predictive of spike timing (*bottom* panels, total of 10 cases). Figure conventions are the same as described in Fig. 2. As with Fig. 2, discontinuities in some of the images are due to omission from the plots of frequencies around 60 Hz.

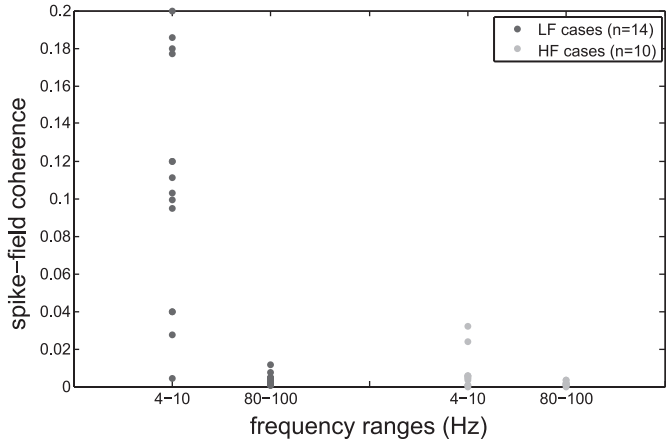

Fig. 8. Spike-field coherence values at 2 different frequency ranges (4–10 and 80–100 Hz) for cells responding to low-frequency LFP (LF cases) and for cells responding to high-frequency LFP (HF cases). Each dot represents 1 recording of unit activity and LFP on the same electrode.

sion, see Zanos 2009). If LFPs do capture averaged synaptic and spiking activity in a small volume of cortical tissue (Katzner et al. 2009), the activity of some cells in that region would be expected to be less "congruent" with the activity of the local population on average.

The relatively low numbers of correctly predicted spikes in low frequencies (Table 1) reflect the loose phase locking of spikes to specific phases of the LFP oscillations, as described by Jacobs et al. (2007) and confirmed in our recordings. The seemingly small proportion of correctly predicted spikes from high LFP frequencies, especially after the removal of spike waveforms, is understandable in light of the high degree of accuracy imposed in the model (1 ms) and the sparse neuronal discharge in human temporal cortex. Since LFPs represent a mixture of multiple local processes, one would expect a significant source of variance to be unrelated to the firing of the recorded cell.

In a number of dual-electrode cases, models capable of predicting timing of unit activity on one electrode from LFP recorded on another nearby electrode were computed. Their performance was inferior to that of the corresponding single-

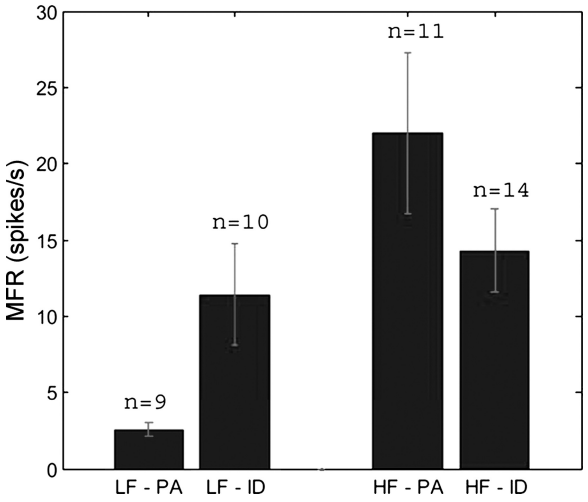

Fig. 9. Mean firing rates (MFR; ± standard mean errors) of the 2 groups of cells (LF and HF) for the 2 different behavioral events: paired associate (PA) and object identification (ID).

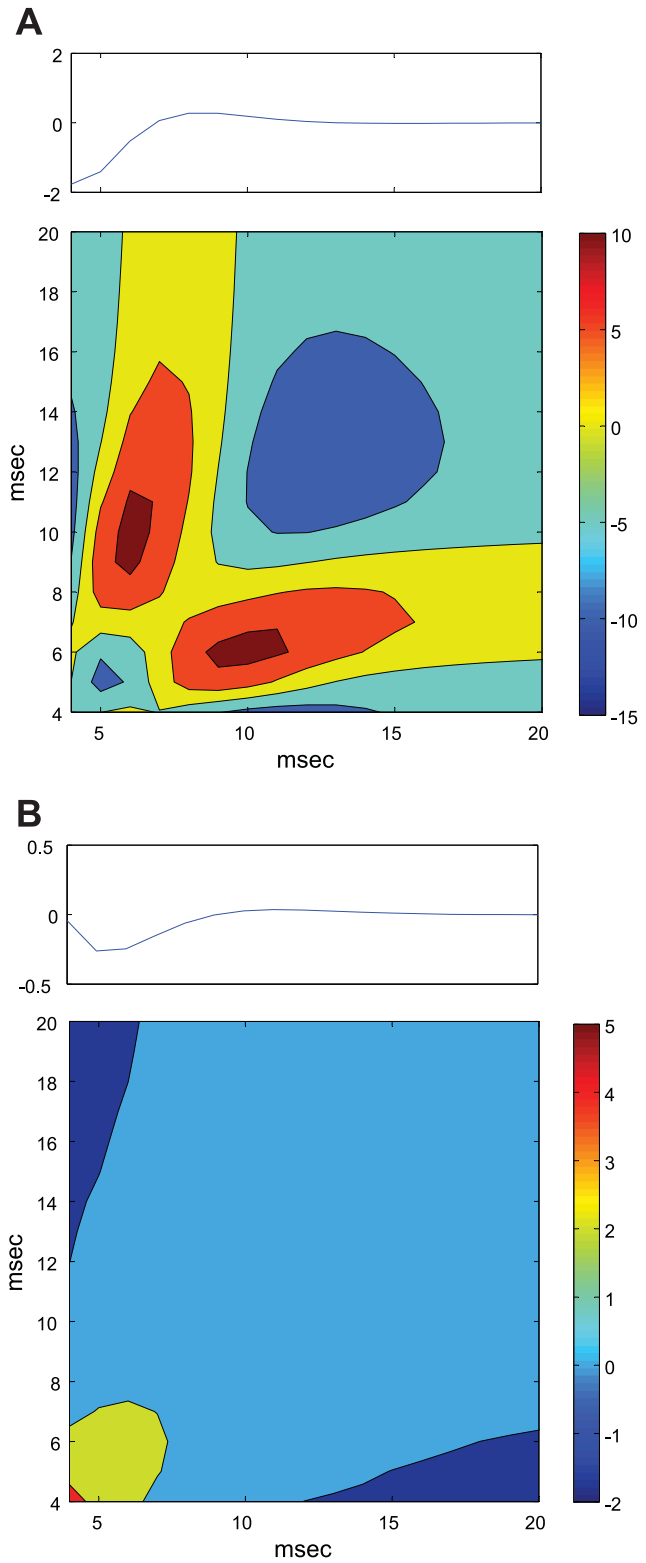

Fig. 10. First- (*top* panels) and second-order (*bottom* panels) kernels for 2 cases where LFP at different frequencies was predictive of spike timing. *A*: a case where LFP at the range of 80–200 Hz was predictive. *B*: a case where LFP at 4–8 Hz was predictive. In both cases, *time 0* corresponds to the occurrence of the spike, and after that the time axis extends in the past (e.g., *time 10 ms* corresponds to 10 ms before the occurrence of the spike). Note that both first- and second-order kernels include positive and negative values.

electrode cases, especially at higher LFP frequencies (Fig. 3). This is not unexpected, given the relatively large distances between the two recording electrodes (average vertical distance 1.1 mm), which are significantly larger than the ~250 μm that the LFP signal is thought to spread (Katzner et al. 2009) . On the other hand, performance of dual-electrode models with lower frequency LFPs is less suppressed, which could be due to the spatial scale of lower frequencies being much larger and, therefore, low-frequency LFPs being more redundant (Steriade 2004).

The non-zero prediction capacity of models computed from dual-electrode recordings indicates that these models capture causal relationships between LFPs and spike timing, because the potential confounding effect of remnants of spike waveforms in the LFP signal is absent. The performance of those models drops to chance levels with increasing LFP frequency > 80 Hz (Fig. 3). That would agree with a gradually decreasing volume of the effect of the LFP on the spiking of neighboring cells with increasing frequency (Destexhe et al. 1999). In that model, a single-electrode recording simply represents the extreme case when even higher frequency LFPs exert an effect on spiking of cells in their immediate vicinity. Whether this model is correct or the performance of single-electrode models is a result of remnants of spike waveforms ultimately depends on how convincing the results of the spike removal process are. Despite the many controls we performed, described above in "*Model Performance,*" there is no definitive method for quantifying how complete spike removal is.

For the seven cells that were recorded for at least two different behavioral blocks, the computed models performed at virtually the same levels for the different behavioral conditions. This means that, at least in those cases, different behaviors were associated with a stable LFP-spike timing relationship. It should be noted, however, that in temporal association cortex, changes in neuronal firing rates and LFP power with different behavioral conditions are modest (Ojemann 2003), and therefore, a stable spike-field relationship may be reflecting that fact.

We also examined the dependence of spike timing on LFP modulations at five different frequency ranges (4–8, 8–14, 14–30, 30–60, and 80–150 Hz). The selection of those ranges was based on the rationale that they reflect different functional and anatomic properties of the underlying neural systems (Buzsaki and Draguhn 2004). We found that significant cases generally fell into one of two groups. In one group, lower LFP frequencies (<14 Hz) were more predictive of spike timing, whereas in the second group, high frequencies (>80 Hz) were more predictive (Fig. 5*A*).

LF cases were associated with weaker nonlinear model components, more common phase locking, and higher SFC values at low frequencies, whereas HF cases had stronger nonlinear model components, less frequent phase locking, and much smaller SFC values at low frequencies (Fig. 5*B*, Table 1, and Fig. 8). In addition, in LF cases, low-frequency LFPs from neighboring electrodes were almost as predictive, in contrast to HF cases (Fig. 3). Cells in the first group tended to be more phase-locked at lower frequencies and fired when high-frequency LFP amplitude was low; cells in the second group tended to be less phase-locked in general and fired when high-frequency LFP amplitude was high (Fig. 7). There is a known interaction between low-frequency phase and high-frequency amplitude in the LFP (Canolty et al. 2006; Cohen et al. 2009; Miller et al. 2010; Mormann et al. 2005). This phase-amplitude coupling could explain the fact that some of the neurons that are "responsive" to high-frequency LFP modulations also show some amount of locking to specific phases of low-frequency LFP. It does not, however, explain the reverse relationship between the occurrence of phase locking to low frequencies and dependence of spike timing on high-frequency amplitude (Fig. 5*B*).

It is known that cortical cells often have a preference for firing at specific phases of ongoing LFP oscillations (e.g., Jacobs et al. 2007; Murthy and Fetz 1996). That linear property of cell firing is captured in our recordings by the models that performed better at lower LFP frequencies and manifests itself in high SFC values at those frequencies (Fig. 8). First-order kernels in those cases show a negative dip that precedes spikes by ~3–5 ms (Fig. 10). That effect might be capturing the refractory period and/or the effect of phase locking of spikes to negative extracellular voltage deflections at that time lag, because a negative kernel acting on negative input results in increased model output. Indeed, spiking of those cells tends to occur at the descending limb of the depolarizing phase of low-frequency LFPs (Fig. 7*A*, *top*).

In those cases where high-frequency (80–150 Hz) LFP was more predictive of spike timing, models instead capture a transient increase in high-frequency LFP power that precedes the spike by approximately a full cycle, i.e., ~10 ms (Fig. 10*A*). Second-order kernels in those cases include two high-frequency LFP components that predict spiking: a full 100-Hz cycle that peaks 10 ms before the spike and that manifests itself in the kernel as the medium-sized peak at 2 and 12 ms, and a bout of increased power, independent of voltage sign, occurring at the same time, seen as a large peak on the main diagonal of the kernel. The first component likely captures the oscillatory nature of the input, whereas the second reflects the fact that the absolute amplitude of the input and not its sign is driving the cell to fire.

What could be the physiological correlate of these two distinct LFP-spiking dependencies? The low-frequency components of the LFP signal are thought to be related to the activity of distant neuronal populations that are connected to the recording site (Belitski et al. 2008; Khawaja et al. 2009). These long-range connections can lock spikes to specific phases of slow LFP oscillations, due to the time lags introduced by synaptic and projection delays. On the other hand, high-frequency components of the LFP may reflect mainly activity from neighboring neuronal circuits (Henrie and Shapley 2005; Khawaja et al. 2009). The 100-Hz wavelet that in this group of cells precedes spikes by approximately a full cycle could be reflecting the temporal summation of local postsynaptic potentials or of correlated multiunit activity from nearby cells (Fetz et al. 1991, 2000; Gray and Viana Di Prisco 1997; Maldonado et al. 2008; Steinmetz et al. 2000). The LF and HF cells could therefore be representing two different populations of neurons in the human temporal cortex that project to (and/or receive projections from) distant and local neuronal populations, respectively.

Even though all cells we recorded from were located in the anterior temporal cortex, the two groups of neurons were active in opposite ways during the two different behavioral tasks, as shown in Fig. 9. LF neurons tended to fire at higher rates

during the ID task, whereas HF neurons preferred the PA task. The ID task is a verbal identification task, whereas the PA task is primarily a verbal learning and memory task. During identification of a stimulus, LF neurons in anterior temporal cortex could be receiving sensory and perceptual input from more distant sources, both temporal and extratemporal. During learning, HF neurons could tend to be driven from more proximal, local neuronal populations in anterior temporal cortex, engaged in memory retention and retrieval. In support of such a model, electrical stimulation studies have provided evidence for involvement of anterior temporal sites in verbal learning, whereas posterior temporal sites were more related to identification (Destexhe et al. 1999; Ojemann et al. 1989; Ojemann 1983, 2003).

We showed that, in many cases, certain LFP components are associated with the timing of neuronal discharge at millisecond resolution. Given that LFPs and unit spiking reflect different aspects of local cortical physiology, Volterra kernels could be used not only to study interrelationships between the various cortical signals but also to probe specific questions about the physiology of local cortical circuits, including interactions between cells and inferring cortical connectivity patterns (Zanos et al. 2008). In addition, a model that assigns LFP features to precise spike timing could be used in spike timing-sensitive applications of LFP-based brain machine interfaces [e.g., spike timing-dependent synaptic plasticity (Jackson et al. 2006)].

ACKNOWLEDGMENTS

We thank E. Lettich, L. Zamora, and J. Schoenfield-McNeill for the intraoperative recordings and A. G. Richardson and S. Perlmutter for helpful discussions.

Present address of T. P. Zanos: Montreal Neurological Institute, McGill University, Montreal, Canada.

GRANTS

This work was supported by National Institutes of Health (NIH) Grant NS12542 (to S. Zanos and E. E. Fetz), NIH Grant P41 EB001978 (to T. P. Zanos and V. Z. Marmarelis), National Science Foundation Grant EEC-0310723 (to T. P. Zanos and V. Z. Marmarelis), and NIH Grant EB2663 (to G. A. Ojemann).

DISCLOSURES

No conflicts of interest, financial or otherwise, are declared by the author(s).

AUTHOR CONTRIBUTIONS

Author contributions: S.Z., G.A.O., and E.E.F. conception and design of research; S.Z. and T.P.Z. analyzed data; S.Z., V.M., G.A.O., and E.E.F. interpreted results of experiments; S.Z. and T.P.Z. prepared figures; S.Z. drafted manuscript; S.Z., T.P.Z., V.M., G.A.O., and E.E.F. edited and revised manuscript; S.Z., T.P.Z., V.M., G.A.O., and E.E.F. approved final version of manuscript; G.A.O. performed experiments.

REFERENCES

Akaike H. Likelihood and the Bayes procedure. In: *Bayesian Statistics*, edited by Bernardo JM. Valencia, Spain: Valencia University Press, 1980, p. 143–166.

Andersen RA, Musallam S, Pesaran B. Selecting the signals for a brain-machine interface. *Curr Opin Neurobiol* 14: 720–726, 2004.

Baker SN, Pinches EM, Lemon RN. Synchronization in monkey motor cortex during a precision grip task. II. Effect of oscillatory activity on corticospinal output. *J Neurophysiol* 89: 1941–1953, 2003.

Belitski A, Gretton A, Magri C, Murayama Y, Montemurro MA, Logothetis NK, Panzeri S. Low-frequency local field potentials and spikes in primary visual cortex convey independent visual information. *J Neurosci* 28: 5696–5709, 2008.

Buzsaki G, Buhl DL, Harris KD, Csicsvari J, Czeh B, Morozov A. Hippocampal network patterns of activity in the mouse. *Neuroscience* 116: 201–211, 2003.

Buzsaki G, Draguhn A. Neuronal oscillations in cortical networks. *Science* 304: 1926–1929, 2004.

Calvin WH, Ojemann GA, Ward AA Jr. Human cortical neurons in epileptogenic foci: comparison of inter-ictal firing patterns to those of "epileptic" neurons in animals. *Electroencephalogr Clin Neurophysiol* 34: 337–351, 1973.

Canolty RT, Edwards E, Dalal SS, Soltani M, Nagarajan SS, Kirsch HE, Berger MS, Barbaro NM, Knight RT. High gamma power is phase-locked to theta oscillations in human neocortex. *Science* 313: 1626–1628, 2006.

Cohen MX, Elger CE, Fell J. Oscillatory activity and phase-amplitude coupling in the human medial frontal cortex during decision making. *J Cogn Neurosci* 21: 390–402, 2009.

Crone NE, Sinai A, Korzeniewska A. High-frequency gamma oscillations and human brain mapping with electrocorticography. *Prog Brain Res* 159: 275–295, 2006.

Destexhe A, Contreras D, Steriade M. Spatiotemporal analysis of local field potentials and unit discharges in cat cerebral cortex during natural wake and sleep states. *J Neurosci* 19: 4595–4608, 1999.

Einevoll GT, Pettersen KH, Devor A, Ulbert I, Halgren E, Dale AM. Laminar population analysis: estimating firing rates and evoked synaptic activity from multielectrode recordings in rat barrel cortex. *J Neurophysiol* 97: 2174–2190, 2007.

Feldman ML. Morphology of the neocortical pyramidal neuron. In: *Cerebral Cortex*, edited by Peters A and Jones EG. New York: Plenum, 1984, p. 123–200.

Fetz EE, Chen D, Murthy VN, Matsumura M. Synaptic interactions mediating synchrony and oscillations in primate sensorimotor cortex. *J Physiol (Paris)* 94: 323–331, 2000.

Fetz EE, Toyama K, Smith W. Synaptic interaction between cortical neurons. In: *Cerebral Cortex*, edited by Peters A and Jones EG. New York: Plenum, 1991, p. 1–47.

Fries P, Reynolds JH, Rorie AE, Desimone R. Modulation of oscillatory neuronal synchronization by selective visual attention. *Science* 291: 1560–1563, 2001.

Gold C, Henze DA, Koch C, Buzsaki G. On the origin of the extracellular action potential waveform: a modeling study. *J Neurophysiol* 95: 3113–3128, 2006.

Gray CM, Viana Di Prisco G. Stimulus-dependent neuronal oscillations and local synchronization in striate cortex of the alert cat. *J Neurosci* 17: 3239–3253, 1997.

Henrie JA, Shapley R. LFP power spectra in V1 cortex: the graded effect of stimulus contrast. *J Neurophysiol* 94: 479–490, 2005.

Hoeffding W. A class of statistics with asymptotically normal distribution. *Ann Math Stat* 19: 293–325, 1948.

Jackson A, Mavoori J, Fetz EE. Long-term motor cortex plasticity induced by an electronic neural implant. *Nature* 444: 56–60, 2006.

Jacobs J, Kahana MJ, Ekstrom AD, Fried I. Brain oscillations control timing of single-neuron activity in humans. *J Neurosci* 27: 3839–3844, 2007.

Kamondi A, Acsady L, Wang XJ, Buzsaki G. Theta oscillations in somata and dendrites of hippocampal pyramidal cells in vivo: activity-dependent phase-precession of action potentials. *Hippocampus* 8: 244–261, 1998.

Katzner S, Nauhaus I, Benucci A, Bonin V, Ringach DL, Carandini M. Local origin of field potentials in visual cortex. *Neuron* 61: 35–41, 2009.

Kelly RC, Smith MA, Samonds JM, Kohn A, Bonds AB, Movshon JA, Lee TS. Comparison of recordings from microelectrode arrays and single electrodes in the visual cortex. *J Neurosci* 27: 261–264, 2007.

Khawaja FA, Tsui JM, Pack CC. Pattern motion selectivity of spiking outputs and local field potentials in macaque visual cortex. *J Neurosci* 29: 13702–13709, 2009.

Maldonado P, Babul C, Singer W, Rodriguez E, Berger D, Grun S. Synchronization of neuronal responses in primary visual cortex of monkeys viewing natural images. *J Neurophysiol* 100: 1523–1532, 2008.

Marmarelis VZ. Identification of nonlinear biological systems using Laguerre expansions of kernels. *Ann Biomed Eng* 21: 573–589, 1993.

Marmarelis VZ. *Nonlinear Dynamic Modeling of Physiological Systems*. New York: Wiley, 2004.

Miller KJ, Hermes D, Honey CJ, Sharma M, Rao RP, den Nijs M, Fetz EE, Sejnowski TJ, Hebb AO, Ojemann JG, Makeig S, Leuthardt EC. Dynamic modulation of local population activity by rhythm phase in human occipital cortex during a visual search task. *Front Hum Neurosci* 4: 197, 2010.

Mitzdorf U. Current source-density method and application in cat cerebral cortex: investigation of evoked potentials and EEG phenomena. *Physiol Rev* 65: 37–100, 1985.

Mormann F, Fell J, Axmacher N, Weber B, Lehnertz K, Elger CE, Fernandez G. Phase/amplitude reset and theta-gamma interaction in the human medial temporal lobe during a continuous word recognition memory task. *Hippocampus* 15: 890–900, 2005.

Murthy VN, Fetz EE. Synchronization of neurons during local field potential oscillations in sensorimotor cortex of awake monkeys. *J Neurophysiol* 76: 3968–3982, 1996.

O'Keefe J, Recce ML. Phase relationship between hippocampal place units and the EEG theta rhythm. *Hippocampus* 3: 317–330, 1993.

Ojemann G, Ojemann J, Lettich E, Berger M. Cortical language localization in left, dominant hemisphere. An electrical stimulation mapping investigation in 117 patients. *J Neurosurg* 71: 316–326, 1989.

Ojemann GA. Brain organization for language from the perspective of electrical stimulation mapping. *Behav Brain Sci* 6: 189–206, 1983.

Ojemann GA. The neurobiology of language and verbal memory: observations from awake neurosurgery. *Int J Psychophysiol* 48: 141–146, 2003.

Ojemann GA, Corina DP, Corrigan N, Schoenfield-McNeill J, Poliakov A, Zamora L, Zanos S. Neuronal correlates of functional magnetic resonance imaging in human temporal cortex. *Brain* 133: 46–59, 2010.

Ojemann GA, Schoenfield-McNeill J. Activity of neurons in human temporal cortex during identification and memory for names and words. *J Neurosci* 19: 5674–5682, 1999.

Penttonen M, Kamondi A, Acsady L, Buzsaki G. Gamma frequency oscillation in the hippocampus of the rat: intracellular analysis in vivo. *Eur J Neurosci* 10: 718–728, 1998.

Quiroga RQ, Nadasdy Z, Ben-Shaul Y. Unsupervised spike detection and sorting with wavelets and superparamagnetic clustering. *Neural Comput* 16: 1661–1687, 2004.

Rasch MJ, Gretton A, Murayama Y, Maass W, Logothetis NK. Inferring spike trains from local field potentials. *J Neurophysiol* 99: 1461–1476, 2008.

Ray S, Crone NE, Niebur E, Franaszczuk PJ, Hsiao SS. Neural correlates of high-gamma oscillations (60–200 Hz) in macaque local field potentials and their potential implications in electrocorticography. *J Neurosci* 28: 11526–11536, 2008.

Schwarz GE. Estimating the dimension of a model. *Ann Stat* 6: 461–464, 1978.

Steinmetz PN, Roy A, Fitzgerald PJ, Hsiao SS, Johnson KO, Niebur E. Attention modulates synchronized neuronal firing in primate somatosensory cortex. *Nature* 404: 187–190, 2000.

Steriade M. Cellular substrates of brain rhythms. In: *Electroencephalography: Basic Principles, Clinical Applications, and Related Fields* (5th ed.), edited by Niedermeyer E and Lopes da Silva FH. Philadelphia, PA: Lippincott Williams & Wilkins, 2004, p. 31–83.

Zanos S. Neural correlates of high-frequency intracortical and epicortical field potentials. *J Neurosci* 29: 3673–3675, 2009.

Zanos TP, Courellis SH, Berger TW, Hampson RE, Deadwyler SA, Marmarelis VZ. Nonlinear modeling of causal interrelationships in neuronal ensembles. *IEEE Trans Neural Syst Rehabil Eng* 16: 336–352, 2008.

Zanos TP, Mineault PJ, Pack CC. Removal of spurious correlations between spikes and local field potentials. *J Neurophysiol* 105: 474–486, 2011.